

Calculated and measured angular correlation between photoelectrons and Auger electrons from K-shell ionization

F Robicheaux¹, M P Jones^{1,2}, M Schöffler^{3,4}, T Jahnke³, K Kreidi³,
J Titze³, C Stuck³, R Dörner³, A Belkacem⁴, Th Weber⁴
and A L Landers¹

¹ Department of Physics, Auburn University, AL 36849, USA

² Department of Physics, Lynchburg College, VA 24501, USA

³ Institut für Kernphysik, J W Goethe-Universität Frankfurt am Main, Max-von-Laue-Str. 1, D-60438 Frankfurt, Germany

⁴ Lawrence Berkeley National Laboratory, Berkeley, CA 94720, USA

E-mail: robicfj@auburn.edu

Received 14 June 2012, in final form 12 July 2012

Published 9 August 2012

Online at stacks.iop.org/JPhysB/45/175001

Abstract

We have applied a recently developed computational method to an experimental puzzle that involves a slow outgoing electron that is scattered by a high-energy Auger electron. Although the experiment seemed to be in a regime accurately described by classical mechanics, such classical calculations could not accurately model the angular distribution of the electron pair. Using the wavefunction from our calculations to generate the energy and angular distributions of the two electrons, we have compared our results to measurements performed at the Advanced Light Source. We have obtained good agreement between the experiment and our quantum results, attributing the poor classical result to the small number of angular momenta in the wavefunction. We have included predictions on how measurements depend on the Auger energy and/or the photoelectron energy.

(Some figures may appear in colour only in the online journal)

1. Introduction

The interaction between two continuum electrons can lead to interesting physical processes. Often, the theoretical or computational treatment of two continuum electrons can be very challenging. An example of an interesting but computationally difficult situation is the angular distribution that results when the two electrons sequentially leave the atom as in [1]. In this experiment, a neon atom absorbs an x-ray so that a 1s electron leaves the atom with ~ 2 eV of energy; after a short time, the Ne core emits an Auger electron of energy ~ 800 eV (~ 29.4 au). The Auger electron has substantially more energy than the photoelectron which means it necessarily passes the photoelectron at a distance depending on the separation of emission times. This gives rise to the possibility for interesting three-body interactions involving the two continuum electrons and the Ne^{2+} ion.

Post collision interaction effects in photoionization have been extensively studied using experimental and/or theoretical methods [2–7]. For the case of Ne, the authors of [4–6] showed that energy shifts and the escape probability for the photoelectron are consistent with the sudden-approximation; in this approximation, the potential of the photoelectron suddenly changes from $-1/r$ to $-2/r$ after the Auger electron is emitted. The electron–electron interaction leads to shifts of the energy distribution of the individual electrons and can even lead to recapture of the photoelectron [8, 9].

The energy distribution of the photoelectron was correctly explained many years ago [10, 11]. Penent *et al* [7] used a technique developed in [12] to measure both of the electron energies in coincidence, showing the correlation between the two energies. Typically, the photoelectron shifts to lower energy and the Auger electron is shifted to higher energy. The changing energy distribution has been described by various

approximate treatments of the electron–electron interaction. However, the angular distribution of the photoelectron relative to the direction of the Auger electron is more difficult to explain because it involves the close approach of two electrons. The angular correlation between the electrons was studied theoretically for the case of equal or nearly equal continuum energies [13, 14]. Scherer *et al* [15] studied this regime in Xe and their results were consistent with the quantum calculations. However, their results were also consistent with classical calculations because the measurements were over a limited angular region.

The new feature of [1] was that the distribution of the electrons with regards to the angle between their emission (or, equivalently, the cosine of this angle) was measured in a region where the approximations in [13, 14] do not apply. Existing quantum theories were derived for the case where all particles are weakly interacting or only one of the pair of particles is strongly interacting [16]. For the case of [1], there were two pairs of strongly interacting particles (the Auger electron with the photoelectron and the photoelectron with the Ne^{2+} core)⁵. In an attempt to understand the measured distributions in [1], a classical trajectory Monte Carlo (CTMC) calculation was performed for the parameters relevant to the experiment. While the energy distribution of the photoelectron was accurately reproduced, the angular distribution in the experiment substantially differed from the CTMC calculation. This was something of a puzzle since both electrons were in the regime where the de Broglie wavelength was small compared to the interaction distances.

In this paper, we extend the numerical treatment of two electrons developed in [17] to describe this system. Robicheaux [17] described how to solve the two-electron Schrödinger equation using a discrete variable representation for the $\cos(\theta_{12})$ operator. In conjunction with a Numerov approximation for the radial coordinates, computing the wavefunction under extreme conditions for the two electrons became possible without needing extreme resources. Extending [17] to treat the sequential electron ejection allows us to quantitatively compare a fully quantum calculation to the measurement. We find good agreement between the calculation and the experimental results. Our main goal is not simply to obtain good agreement between measurements and calculations but also to understand the origin of the features measured. Another important goal is to use the calculation to understand the trends of this system and to predict how the measurements depend on physical parameters.

We compare our calculations to new experimental results obtained at the Advanced Light Source. As in [1], we used cold target recoil ion momentum spectroscopy (COLTRIMS) to study the continuum correlation between the photoelectron of core-photoionized neon and the subsequent Auger electron. The experimental technique was essentially identical to

that in [1] except we used circularly polarized photons at slightly higher energy. We simultaneously measured both the photoelectron (directly) and the Auger electron (indirectly) following core photoionization of neon at 1.99 eV (~ 0.073 au) above threshold; the present measurements have much better statistics than [1].

Atomic units are used except where explicitly noted otherwise.

2. Basic theory

This section describes the numerical method we used to compute physical properties of this system. We recast the time-dependent Schrödinger equation for the problem of a photoelectron with the subsequent Auger decay as three coupled channels: (1) photoelectron with a $1s2s^22p^6$ core, (2) photoelectron plus photon with $1s^22s^22p^5$ core, and (3) photoelectron plus the Auger electron with $1s^22s^22p^4$ core. Since channels 2 and 3 do not interact and channel 1 irreversibly decays into channels 2 and 3, we can use second-order perturbation theory to formally eliminate the coupling [18].

For the experimental results below, the most important part of the interaction occurs when both electrons are well outside of the core region. This allows two approximations which only slightly change the computed results but lead to a vast simplification. The first change was to use total $L = 0$ wavefunctions for the outgoing two-electron wavefunction instead of $L = 0, 1, 2,$ or 3 for the actual atom. The total angular momentum of the Ne wavefunction is $L = 1$ since it is a single photon transition from the ground state, but the Ne^{2+} core can have angular momentum which means that the total angular momentum of the outgoing pair can have the range $0-3$. This allows us to decrease the coupled channels by a large factor and should be accurate since the electron–electron interaction occurs over large distances (100 or more au). The other change was to approximate the Auger decay as a separable function which is only inaccurate for the part of the wavefunction with both electrons inside ~ 2 au; since the photoelectron has an average r of ~ 50 au when the Auger decay occurs, this should also be a good approximation.

2.1. Reformulation into inhomogeneous Schrödinger equation

In this section, we reformulate the time-independent Schrödinger equation into a time-dependent equation with a source term. This time-dependent Schrödinger equation contains the $1/r_{12}$ operator and, thus, is not perturbative with respect to the interaction between the photoelectron and Auger electron. As described at the end of this section, the approximation with our method is due to an incorrect treatment of the two continuum electrons when *both* electrons are within ~ 1 au of the nucleus. For the case considered in this paper, the Auger electron is typically emitted when the photoelectron is far from the nucleus; thus, this should be a good approximation.

We first derive the effect of the Auger decay on the part of the wavefunction relevant to the photoelectron. Gorczyca and Robicheaux [18] extended the application of [19] to the

⁵ For example, equation (26) of the second part of [16] is a direct derivation from equation (21) of the first part of [16]. To be valid, the conditions in equation (16a) of the first part of [16] must hold. For the situation in [1] and this paper, this means |PE| between either electron and the Ne^{2+} ion must be much less than their KE. In [1], the |PE| was larger than the KE and in this paper this means that the part of the wavefunction with $r < 30$ au for the photoelectron has |PE| greater than the KE.

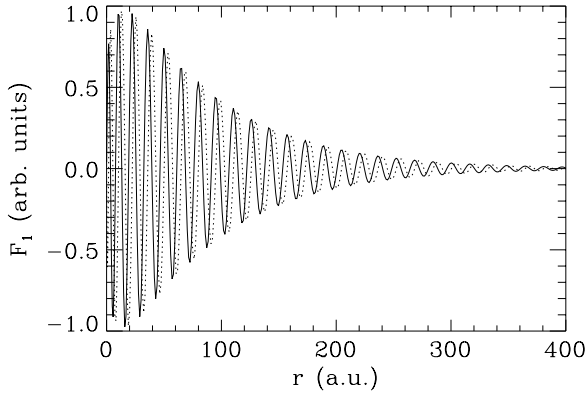


Figure 1. The real (solid line) and the imaginary (dotted line) parts of the $F_1(r)$ function of equation (2) for an energy of 0.0735 au (2 eV) and a width of 0.01 au (270 meV).

optical potential relevant to the decay of a core state when a Rydberg electron is outside of the region of space defined by the core electrons. Although the treatment of [18] was for a Rydberg electron outside of a core that could emit an Auger electron, this treatment will work just as well for a continuum electron outside of a core that can emit an Auger electron. The main result is that the core energy is replaced by a complex core energy

$$E_c \rightarrow E_c - i \frac{\Gamma_c}{2}, \quad (1)$$

where Γ_c is the energy width of the core.

Once the atom absorbs a photon there will be a part of the wavefunction corresponding to the outgoing photoelectron with an undecayed core and a part of the wavefunction that corresponds to a double electron continuum (both the photoelectron and the Auger electron emitted). The treatment of [18] leads to an equation for the wavefunction corresponding to the outgoing photoelectron with the core *not* decayed:

$$\left(E - E_c + i \frac{\Gamma_c}{2} - H_a \right) F_1 = D\phi_g, \quad (2)$$

where E is the total energy of the system, the $D\phi_g$ is the dipole operator acting on the orbital that absorbs the photon and H_a is the Hamiltonian for the photoelectron. At distances outside of the core, the potential in H_a goes to $-1/r$. For the cases treated in this paper, the exact form of H_a or $D\phi_g$ for distances within the core only changes the normalization of the final result. Since we are not interested in this quantity, the potential in H_a can be taken to be $-1/r$ for *all* distances and the $D\phi_g$ can be taken to be any short range function with the correct angular momentum as long as it is *not* an eigenstate of the H_a used.

Figure 1 shows the real and imaginary parts of $F_1(r)$ for a photoelectron at 0.0735 au (2 eV) and with $\Gamma_c = 0.01$ au (270 meV). The trends in the function $F_1(r)$ can be understood qualitatively. As the width Γ_c increases, the radial extent of F_1 decreases because the decay occurs more quickly. As the real part of the energy increases, the wavelength becomes smaller and the radial extent of F_1 increases. The radial extent increases because the photoelectron is faster at higher energy and, thus, can reach larger distances before the core decays. The average value of r for the case in figure 1 is 49 au which is one measure indicating the photoelectron is well outside of the core before

the Auger decay occurs. The fraction of the wavefunction at distances larger than 2 au is $\sim 98\%$ which is the percentage of the wavefunction that corresponds to the condition that the photoelectron is outside of the core region when the Auger decay occurs.

We can use the $F_1(r_1)$ function as part of the source term for the two-electron wavefunction corresponding to both the photoelectron and Auger electron in the continuum. From [19], the outgoing wave corresponding to the two-electron continuum can be written as

$$\Lambda = \frac{1}{E - H} [F_1 V_{\text{opt}} \Phi_c], \quad (3)$$

where H is the two-electron Hamiltonian and $V_{\text{opt}} \Phi_c$ is the optical potential for the Auger decay acting on the core wavefunction Φ_c . The function Λ has outgoing conditions for both electrons. Because the F_1 extends to such large distances compared to the size of the core, the exact form of the orbital resulting from $V_{\text{opt}} \Phi_c$ is not relevant. It is only necessary that the orbital have the correct angular momentum and be nonzero only in the core region. As with above, the exact form of $V_{\text{opt}} \Phi_c$ strongly affects the normalization of Λ but hardly affects the energy and/or angular distributions.

With equation (3), we have reduced the problem to the solution of an inhomogeneous Schrödinger equation. This is not a simple task due to the large region of space covered by the photoelectron and the relatively high energy of the Auger electron. Instead of the time-independent equation, we use Green's function technique of [20] to recast equation (3) into the time-dependent equation:

$$i \frac{\partial \Lambda}{\partial t} - H \Lambda = S(t) F_1(\vec{r}_1) F_2(\vec{r}_2), \quad (4)$$

where H is the two-electron Hamiltonian and we have replaced $V_{\text{opt}} \Phi_c$ by the short-range function F_2 and the strength of the source $S(t) = 1/(1 + \exp[10\{1 - 5t/t_f\}])$. The parameter t_f is the final time of the calculation. Formally, $S(t)$ should be a step function $S(t) = 0$ for $t < 0$ and $S(t) = 1$ for $t > 0$; however, we found that results converged much better when the step function is rounded off as in [20].

The last important step is to describe how to extract physical parameters from the function Λ . Robicheaux *et al* [20] discussed that the important quantities are the *rate* of change of the properties calculated from the Λ function. For example, the energy distribution is obtained by computing the numerical *time derivative* of the probability $|\langle \Lambda | f_{E_1} f_{E_2} \rangle|^2(t)$ where the continuum functions are energy normalized.

Lastly, we stress that we implemented the methods of this section in an approximate manner. If we had used the exact $D\phi_g$ and $V_{\text{opt}} \Phi_c$ in the source terms and the exact non-local two electron H , then the treatment of this section would be exact except for numerical approximations needed to solve the differential equations. We have deliberately made the choice to approximate the $D\phi_g$ and $V_{\text{opt}} \Phi_c$ by simple short-range functions. The total norm strongly depends on the choice of these functions, but the angular or energy distribution only weakly depends on the two functions; the reason is that the error in the two electron is from when the source has both electrons within $\sim 1 - 2$ au of the nucleus. As long as both functions were of short range and *not* an eigenstate of the Hamiltonian, the distributions were uncertain at the per cent level.

2.2. Numerical method

We use the method described in [17] to numerically solve the inhomogeneous time-dependent Schrödinger equation. As described in [17], we use an implicit algorithm to solve the time-dependent equation. With the source term the sequence of operations that moves Λ forward one time step is as follows:

$$\begin{aligned} \Lambda &= \Lambda - \frac{1}{2}i\delta t S(t) F_1(\vec{r}_1) F_2(\vec{r}_2) \\ \Lambda &= U_1(\delta t) U_2(\delta t) \Lambda \\ \Lambda &= \Lambda - \frac{1}{2}i\delta t S(t + \delta t/2) F_1(\vec{r}_1) F_2(\vec{r}_2) \\ \Lambda &= U_3(\delta t) \Lambda, \end{aligned} \quad (5)$$

where the implicit propagator

$$U_j(\delta t) = \frac{1 - iH_j\delta t/2}{1 + iH_j\delta t/2} \quad (6)$$

uses $H_3 = 1/r_{12}$ and the one-electron Hamiltonians $H_1 = p_1^2/2 - 2/r_1 - E_1$ and $H_2 = p_2^2/2 - 2/r_2 - E_2$ are shifted in energy so the time steps can be larger; the energies have the condition that the total energy $E = E_1 + E_2$.

The implicit algorithm allows time steps to be more nearly related to the physical timescale of the problem instead of being related to the angular momentum and the grid spacing as with an explicit method. In all of the calculations below, we used $\delta t = 0.24$ au, but we made tests with $\delta t = 0.12$ au; the excellent agreement with the test calculations indicates that we could have used a δt larger than 0.24 au. As in equation (3) of [21], the wavefunction is represented by a superposition over coupled angular momenta with ℓ_1 and ℓ_2 coupled to total L and the spins coupled to total S ; we also represent the radial functions using a grid of points. The action of the U_1 and U_2 operators on the wavefunction is easy to evaluate because the H_1 and H_2 operators are diagonal in ℓ and are taken to be tridiagonal in r . The U_1 and U_2 propagators were implemented using both a simple three-point difference and with a higher order Numerov approximation; the Numerov approximation gave converged results with less than 1/2 the number of points of the simple three-point difference [17].

The main difficulty to overcome in [17] was the action of the U_3 operator on the wavefunction. We borrowed an idea from discrete variable representation to evaluate the action of U_3 [22]. We use our coupled angular momentum states as the orthonormal basis states $|i\rangle = |(\ell_1, \ell_2)L\rangle$ and the $\cos(\theta_{12})$ operator as the coordinate. We tested for convergence by increasing the maximum ℓ in the calculation. We found that $\ell_{\max} = 10$ gave results that were converged except near $\cos(\theta_{12}) = 1$. To obtain convergence for all angles, we needed $\ell_{\max} = 15$, although we performed test calculations for $\ell_{\max} = 20$ and 25 as well.

3. Results

Unless stated otherwise, the photoelectron in the calculations will have an energy of 0.0735 au (2 eV) and a width of 0.01 au (270 meV). The width matches that for the 1s hole of Ne. The energy was chosen to closely match that for the measurements made at the Advanced Light Source.

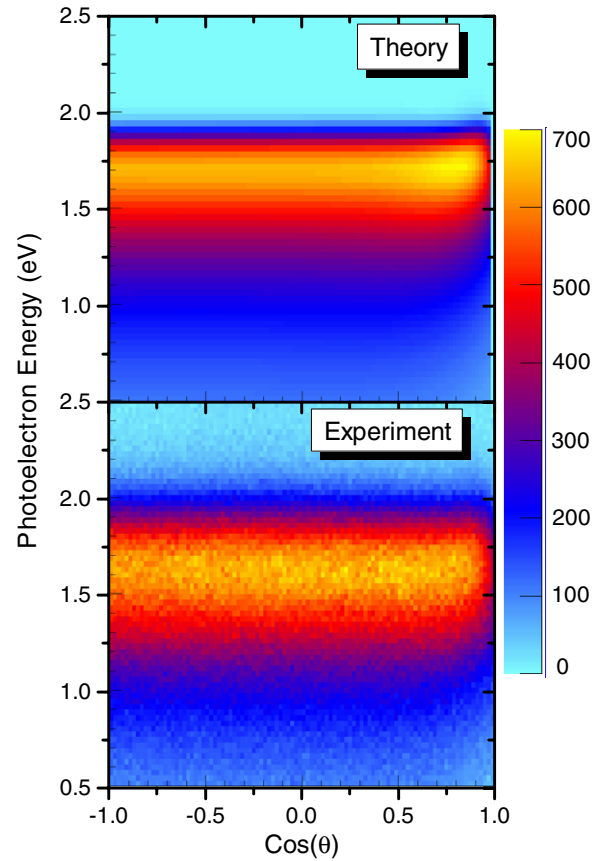


Figure 2. The calculated and experimental photoelectron signal as a function of the photoelectron energy and the cosine of the angle between the photoelectron’s momentum and the Auger electron’s momentum. All other variables (e.g. Auger electron’s momentum) have been integrated over.

Figure 2 shows the photoelectron distribution with respect to energy and cosine of the angle between the momentum vectors of the photoelectron and the Auger electron. The theory graph does not take into account the resolution associated with the electron measurement or the synchrotron photon. We present the results in this form to show that the overall correlation between photoelectron energy and $\cos(\theta)$ is very similar for theory and experiment. There are a couple of generic features that have been understood for many years. The photoelectron energy is shifted down from the initial outgoing energy of 1.99 eV by a clear amount. This has been well explained by the idea that the photoelectron originally has its energy defined with respect to a potential energy of $-1/r$, but after the Auger electron is emitted it suddenly experiences a $-2/r$ potential; this additional binding leads to a shift down in the energy by $1/r$. Since the photoelectron can be in a range of radial distances when the Auger electron is emitted, there is not a single shift but a distribution which is reflected in the final spread in energies. The width of the photoelectron energy distribution also reflects the energy width of the Auger state; the total energy is fixed which means the energy uncertainty of the Auger electron gets mapped onto the photoelectron energy as well. Both of these effects are contained in the quantum calculation and agree very well with the measurement. These

effects have been described in detail [10, 11] and, therefore, we do not present those results here.

The more interesting aspect of figure 2 is where there is correlation between the two variables. In both plots, there is little dependence with respect to $\cos(\theta)$ except near $\cos(\theta) = 1$ and the effect is larger when the photoelectron energy is smaller. This correlation arises because the photoelectrons with the largest energy shift are those that are closer to the ion when the Auger electron is ejected; thus, there is more interaction between the electrons which leads to the photoelectron more strongly pushed away from $\cos(\theta) = 1$. A less obvious feature is that the photoelectron distribution for energies between 1.75 and 2 eV does *not* have the probability decrease monotonically with increasing $\cos(\theta)$. There is a small range of $\cos(\theta)$ between ~ 0.8 and 0.95 where the distribution increases giving a small hump just below $\cos(\theta) = 1$. This effect is very pronounced in classical calculations and arises because the photoelectron gets pushed from $\cos(\theta) \simeq 1$ to slightly smaller values which leads to a small peak in probability. The properties of figure 2 near $\cos(\theta) = 1$ seem to arise from the competition between diffraction of the photoelectron (which tends to spread probability in $\cos(\theta)$) and the repelling force between the two electrons which leads to a perfect hole in the distribution at $\cos(\theta) = 1$. Below, we will discuss this effect from a somewhat different perspective.

Figure 3 shows a comparison between the measurements and two different calculations of the photoelectron distribution with respect to $\cos(\theta)$. We restrict the energy range of the photoelectron to be between 0.5 and 2.5 eV because there is a capture re-emission line in the data near 0.3 eV. The previous result in [1] showed that the classical calculation did not match the experiment and our present calculations show similar disagreement with the CTMC results. We think that this is interesting disagreement because the quantum wavefunction has many nodes over the relevant region and the angular distribution involves averaging over all but one of the wavefunction's degrees of freedom. Thus, this system seems ripe for a classical treatment but clearly there is some strongly non-classical property of this system. We will address this below.

The good agreement between the fully quantum calculation and the measurement argues that the quantum

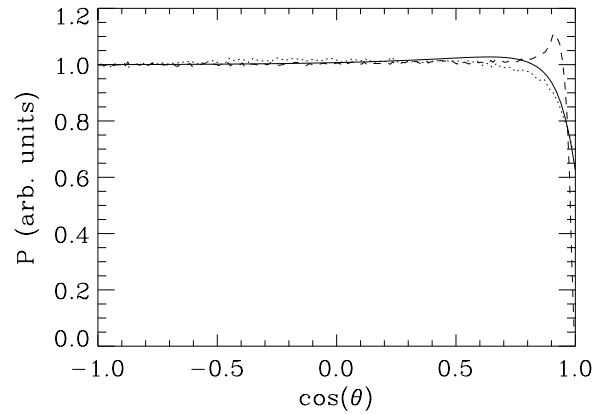


Figure 3. The photoelectron signal as a function of the cosine of the angle between the photoelectron's momentum and the Auger electron's momentum. The photoelectron energy has been integrated over from 0.5 to 2.5 eV and all other variables have been fully integrated over. Solid line is experiment, dotted line is quantum calculation, and the dashed line is the CTMC calculation.

calculation is accurately capturing the relevant physics of this system. However, there is a slight disagreement which could be due to three possibilities. First, the calculation was performed for total $L = 0$ whereas the actual two-electron wavefunction is a superposition of states with the two outgoing electrons coupled to $L = 0, 1, 2$ or 3 . Second, the wavefunction is only accurate when neither electron is within ~ 1 au of the nucleus; perhaps a small correction to the wavefunction in this region would increase the agreement. Third, the experiment could have slight systematic errors, limited statistics, or limited resolution that leads to the difference; for example, there are a couple of capture re-emission lines which could affect the angular distribution at this level.

Figure 4 shows how the angular distribution evolves with the Auger energy, keeping the photoelectron energy fixed at 0.0735 au (2 eV) and the Auger width at 0.01 au (270 meV). Both of the quantum and the classical calculations show a similar trend although the detailed results differ. As the energy of the Auger electron is decreased, the angular range where there is depleted probability is increased and the range where there is increased probability becomes larger. In

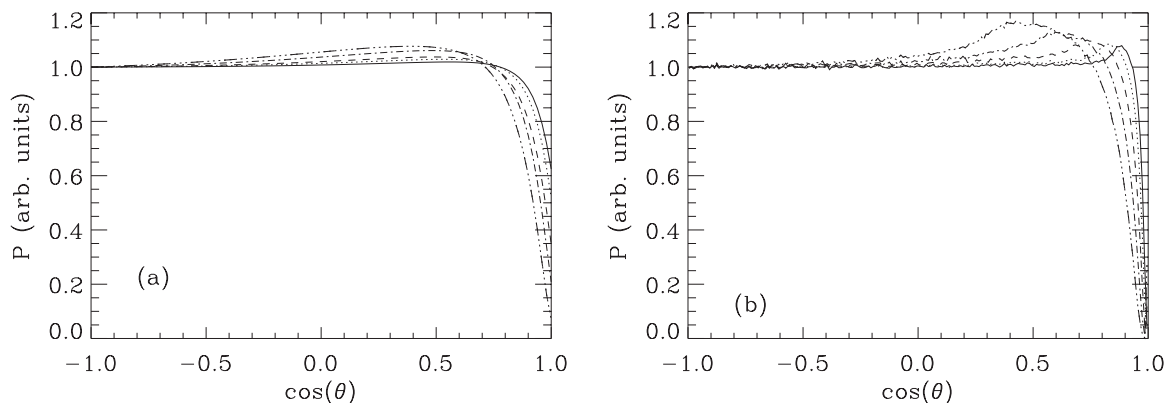


Figure 4. Same as figure 3 except the photoelectron energy is integrated over from 0 to 2.5 eV. All lines are from calculations using different Auger energies. Solid line is for 800 eV (29.4 au), dotted line is for 16 au, dashed line is for 8 au, dash-dot line is for 4 au and dash-dot-dot-dot is for 2 au. Figure (a) is the quantum calculation and (b) is the CTMC calculation.

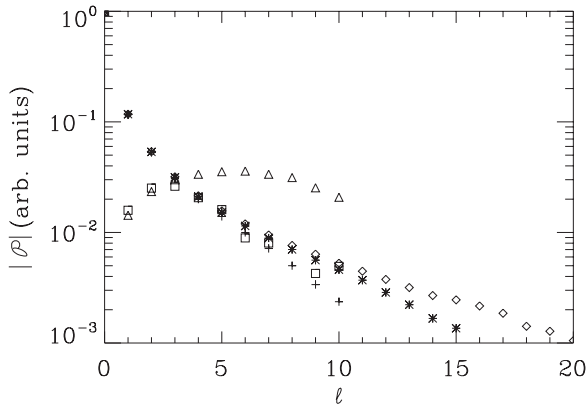


Figure 5. The squares show the Legendre transform of the quantum photoelectron angular distribution and the triangles are the transform of the CTMC results. The + is the square root of the quantum population as a function of ℓ for a calculation with $\ell_{\max} = 10$, the * is the same for a calculation with $\ell_{\max} = 15$, and the diamonds are the same for a calculation with $\ell_{\max} = 20$.

the classical calculation, there is always zero probability for $\cos(\theta) = 1$ because the fast Auger electron always scatters the photoelectron out of its path. The quantum calculation does not give zero probability for the electrons coming out in the same direction; however, as the Auger energy decreases, the probability at $\cos(\theta) = 1$ decreases. By changing to different atomic/molecular systems, the Auger energy can be controlled. Thus, it might be possible to see this trend experimentally.

We also performed calculations where we kept the Auger energy fixed and varied the photoelectron energy from 0.05 to 0.30 au (1.36–8.16 eV). We found that the angular distribution for the photoelectron energy between 0.1 and 0.3 au did not strongly differ. The results for the 0.05 au calculation gave stronger scattering which led to a somewhat deeper dip at $\cos(\theta) = 1$ and a somewhat larger peak in the angular distribution. It is understandable that the 0.05 au calculations gave the largest scattering because the distance the photoelectron travels before the Auger decay decreases with decreasing energy; thus, the 0.05 au case will have the largest electron–electron interaction.

4. Source of classical error

Using the quantum wavefunction, we can address the question about why the quantum calculation differs from the classical calculation, which we found to be somewhat surprising. The wavelength of the Auger electron and photoelectron in the $-1/r$ potential is short enough that both electrons have several wavelengths in the physically relevant region. We show in figure 5 the magnitude of the Legendre polynomial transform of the quantum and classical results and the square root of the ℓ -probability in our wavefunction. The Legendre polynomial transform is defined as

$$\mathcal{P}_\ell = \sqrt{2\ell + 1} \int_0^\pi P_\ell(\cos \theta) P(\cos \theta) \sin \theta \, d\theta, \quad (7)$$

where $P(\cos \theta)$ is the population as a function of θ . We have normalized all of the results to 1 for the $\ell = 0$ component. We have only shown the classical and quantum transforms

out to $\ell = 10$ because fluctuation noise in the classical calculation leads to questionable results for larger ℓ . The classical and quantum transforms give similar values for $\ell \leq 3$, but differ strongly for higher ℓ with the classical transform having substantially more population in higher ℓ . This is understandable because the larger population in higher ℓ is necessary to obtain a sharp angular feature in the classical population and it is the lack of these angular momenta in the quantum calculation that leads to the smaller variation in population near $\cos(\theta) = 1$. Also shown in the figure is the square root of the population for three different calculations: $\ell_{\max} = 10, 15$ and 20 . Since most of the quantum population is in $\ell = 0$, the Legendre transform of the quantum calculation will be approximately proportional to the amplitude $\ell = 0$ times the amplitude in ℓ . For $\ell \geq 3$, the Legendre transform of the quantum results tracks the amplitude for the quantum wavefunction to have that ℓ . Thus, the lack of population in the higher angular momentum in the quantum wavefunction is the reason why the classical calculation does not give quantitative agreement with the quantum calculation. As a side note, we found that the most difficult point to converge in the quantum calculation was $\cos \theta = 1$. As ℓ_{\max} increased, the population at $\cos \theta = 1$ decreased until convergence was achieved because the smaller ℓ_{\max} calculations had the population as a function of ℓ decreases too quickly.

Another way to interpret this result is that the diffraction of the electron wavefunction causes the fine structure in the classical calculation to be blurred. The scattering of the two electrons leads to a hole in the wavefunction where $r_1 = r_2$. As the energy of the Auger electron increases, the size of this hole decreases because the distance of closest approach scales like $1/E$. However, the wavelength of electron 1 is roughly fixed. Thus, the hole at $\cos(\theta_{12}) = 1$ can be filled by diffraction for the higher Auger energies. The two interpretations of the limitations of the classical calculations seem to be completely different but are actually the same thing. The small number of ℓ in the wavefunction is the basis set realization of the wave diffraction in $\cos(\theta_{12})$.

5. Summary

We performed fully quantum calculations for the situation where a slow photoelectron interacts with a much higher energy Auger electron which is emitted from the atom a few femtoseconds after the photoelectron is launched. We obtained good agreement with experimental results. We used the calculated wavefunction to understand why classical calculations did not give a good representation of the experiment.

The results of this paper gives the first successful comparison of the method in [17]. The method we used to propagate the wavefunction is suited to handle situations where the two-electron wavefunction needs many angular momentum, covers a large region of space and/or needs very long time propagation. We plan to adapt the calculations to other situations (e.g. two interacting Rydberg electrons) which could give trouble to other methods.

Acknowledgments

This work was supported by the Chemical Sciences, Geosciences, and Biosciences Division of the Office of Basic Energy Sciences, US Department of Energy (contract nos DE-FG02-00ER15069, DE-AC02-05CH11231 and DE-FG02-10ER16146), by the Deutsche Forschungsgemeinschaft, DAAD, and by a grant of high performance computing resources and technical support from the Alabama Supercomputer Authority. We thank the staff of the Advanced Light Source for outstanding support, in particular, by H Bluhm and T Tylliszczak from beamline 11.0.2.1.

References

- [1] Landers A L *et al* 2009 *Phys. Rev. Lett.* **102** 223001
- [2] Kuchiev M Yu and Sheinerman S A 1989 *Sov. Phys. Usp.* **32** 569
- [3] Sheinerman S A, Lablanquie P and Penent F 2007 *J. Phys. B: At. Mol. Opt. Phys.* **40** 1889
- [4] De Fanis A *et al* 2004 *Phys. Rev. A* **70** 040702
- [5] De Fanis A *et al* 2005 *J. Phys. B: At. Mol. Opt. Phys.* **38** 2229
- [6] Hergenbahn U *et al* 2005 *J. Phys. B: At. Mol. Opt. Phys.* **38** 2843
- [7] Penent F *et al* 2008 *J. Phys. B: At. Mol. Opt. Phys.* **41** 045002
- [8] Gorczyca T W *et al* 2003 *Phys. Rev. A* **68** 050703
- [9] Hentges R *et al* 2004 *J. Phys. B: At. Mol. Opt. Phys.* **37** L267
- [10] King G C, Read F H and Bradford R C 1975 *J. Phys. B: At. Mol. Phys.* **8** 2210
- [11] Russek A and Mehlhorn W 1986 *J. Phys. B: At. Mol. Phys.* **19** 911
- [12] Eland J H D *et al* 2003 *Phys. Rev. Lett.* **90** 053003
- [13] van der Straten P, Morgenstern R and Niehaus A 1988 *Z. Phys. D* **8** 35
- [14] Sheinerman S A and Schmidt V 1997 *J. Phys. B: At. Mol. Opt. Phys.* **30** 1677
- [15] Scherer N *et al* 2004 *J. Phys. B: At. Mol. Opt. Phys.* **37** L121
- [16] Kuchiev M Yu and Sheinerman S A 1988 *J. Phys. B: At. Mol. Opt. Phys.* **21** 2027
- [16] Kuchiev M Yu and Sheinerman S A 1994 *J. Phys. B: At. Mol. Opt. Phys.* **27** 2943
- [17] Robicheaux F 2012 *J. Phys. B: At. Mol. Opt. Phys.* **45** 135007
- [18] Gorczyca T W and Robicheaux F 1999 *Phys. Rev. A* **60** 1216
- [19] Robicheaux F, Gorczyca T W, Pindzola M S and Badnell N R 1995 *Phys. Rev. A* **52** 1319
- [20] Robicheaux F, Pindzola M S and Plante D R 1997 *Phys. Rev. A* **55** 3573
- [21] Pindzola M S *et al* 2007 *J. Phys. B: At. Mol. Opt. Phys.* **40** R39
- [22] Harris D O, Engerholm G G and Gwinn W D 1965 *J. Chem. Phys.* **43** 1515